

DIPPED MAGNETIC FIELD CONFIGURATIONS ASSOCIATED WITH FILAMENTS AND BARBS

D. H. MACKAY, A. W. LONGBOTTOM and E. R. PRIEST

School of Mathematical Sciences, University of St. Andrews, St. Andrews, Fife, Scotland, KY16 9SS

(Received 15 May 1998; accepted 27 October 1998)

Abstract. In this paper, three-dimensional linear force-free field configurations that can be associated with filaments are considered. It is assumed that the field configurations are suitable to represent filaments if they contain magnetic dips. With the photospheric flux distribution chosen to be an arcade with a dextral/sinistral axial component, it is found that dipped configurations exist only for large values of α (where, $\nabla \times \mathbf{B} = \alpha \mathbf{B}$). The dips always lie above the polarity inversion line in the centre of the channel between the flux regions. When the dips are viewed from above to a depth of 1 Mm they resemble closely the shape of filaments viewed in absorption on the solar disk. As the magnitude of α increases, the horizontal and vertical extent of the dips also increases, giving active-region filaments for low values of α and quiescent filaments for high values of α . Dextral filaments only form for negative values of α and sinistral filaments for positive values of α . The portion of the field line that is dipped is always of inverse polarity and the magnitude of the field in the dipped region increases with height, both of which are consistent with Leroy, Bommier, and Sahal-Br  chot (1983). Overlying the region of dips there are arcades of normal polarity which have the correct left-bearing/right-bearing orientation for dextral/sinistral filaments. When the hypothesis of barbs occurring in dipped field lines is used, barbs that branch out of the main axis and to the right/left for dextral/sinistral filaments can be formed around minority polarity elements on either side of the polarity inversion line. No barbs are found around normal polarity elements. The model reproduces many of the observed features of filament channels, filaments and their barbs.

1. Introduction

Solar filaments or prominences are beautiful but mysterious objects. They exist in the solar corona but possess temperatures 500 times less than typical coronal values and densities nearly 100 times greater. Filaments are situated in the corona and their magnetic fields are thought to support the dense mass against gravity and insulate it from the surrounding material (Tandberg-Hansen, 1974). On the Sun there are many different types of prominence or filament (Martin *et al.* 1995), but they can be broadly classified into two main types: quiescent prominences and active region prominences. Quiescent prominences are found at high latitudes on the Sun, such as around the polar crown and exist in quiet background flux regions. In contrast, as their name suggests, active-region prominences form in active-region belts of the Sun and therefore form in regions of strong flux. Although the two types of prominence form in very different environments they always form above locations called Polarity Inversion Lines (P.I.L.). Polarity Inversion Lines lie between regions



Solar Physics **185**: 87–112, 1999.

© 1999 Kluwer Academic Publishers. Printed in the Netherlands.

of opposite polarity flux and denote the location where the vertical component of magnetic field changes sign. Although filaments form above P.I.L.'s the P.I.L. must also be situated in a 'filament channel' (Foukal, 1971; Martin, 1990). A filament channel is a path in the chromosphere characterised by chromospheric fibrils on either side of the P.I.L. that are (i) nearly parallel to one another and (2) nearly parallel to the path of the P.I.L. Filament channels are more fundamental than the filaments that form within them and a single channel can survive successive filament formations and eruptions.

As well as forming in a wide variety of locations, filaments also come in a wide range of sizes with lengths from 60 000–600 000 km, heights 10 000–100 000 km, and widths of 4000–15 000 km (Tandberg-Hansen, 1974). In each of these cases the lower bound corresponds to active-region filaments and the upper bound to quiescent filaments. When magnetic field measurements of prominences are made at the limb the magnetic field strength within a prominence lies between 2–30 G, average 8 G (Athay *et al.*, 1983; Leroy, Bommier, and Sahal-Br  chot, 1983; Querfield *et al.*, 1985). These measurements show that within the prominence the magnetic field is mainly horizontal and makes an angle of 10° – 40° with the prominence axis. The measurements also show that the magnetic field strength is observed to increase with height through the prominence.

In the past, many 2-D models have been put forward for prominences and these can be broadly classified into two categories, those of 'normal polarity' and those of 'inverse polarity' (Priest, 1989). An example of a normal polarity prominence model is that of Kippenhahn and Schl  ter (1957) or Hood and Anzer (1990). It is described as being of normal polarity since the magnetic field threading through the prominence passes over the P.I.L. in the same direction as that of the overlying potential arcade. On the other hand, in an inverse polarity model the magnetic field threading through the prominence passes over the polarity inversion line in a direction opposite to that of the potential arcade, such as in the Kuperus and Raadu (1974) model. Most prominences are observed to be of inverse polarity type (Bommier and Leroy, 1997).

These properties of filaments have been known for many years, but more recently Martin, Bilimoria, and Tracades (1994) found a surprising hemispheric pattern for filament channels and filaments. To begin with, it was found that quiescent prominences are predominantly dextral in the northern hemisphere and sinistral in the southern. A dextral/sinistral filament is one in which the axial magnetic field component points to the right/left when viewed from the positive polarity side. This is surprising since an axial component created by (the obvious cause) differential rotation would give exactly the opposite orientation in each hemisphere. To try and explain this, many new theories have been put forward such as those by Rust and Kumar (1995), Priest, van Ballegooijen, and Mackay (1996), Kuperus (1996), Zirker *et al.* (1997), and Mackay *et al.* (1998). Along with the hemispheric pattern, Martin, Bilimoria, and Tracades (1994) also found that dextral filaments have barbs that are always right-bearing and correspondingly in sinistral filaments they are

always left-bearing. As well as there being a one-to-one correspondence between filaments and barbs there is another between filaments and their overlying arcades. Martin and McAllister (1995) found that stationary arcades above dextral filaments are always left-bearing, while those above sinistral filaments are always right-bearing (as seen from above). Also post-eruption arcades that reform at successive heights above dextral filaments do so with an anti-clockwise rotation with height and above sinistral filaments with a clockwise rotation with height. These patterns show that filament channels and filaments have a well defined magnetic orientation with height and also with location on the Sun.

In the past, few 3-D models of filaments have been constructed. However, Aulanier and Démoulin (1998) formed dipped magnetic configurations in a twisted flux rope by adding specific 3-D harmonics of a linear force-free field and Antiochos, Dahlburg, and Klimchuk (1995) formed dips by shearing and relaxing an initially potential dipole. In this paper, three-dimensional models of magnetic field configurations that can be associated with filament channels and filaments will be constructed. As with previous studies a configuration will be considered suitable if it contains dips in which cool plasma could be held in static support. To begin with, in Section 2 the assumptions of the modelling are given and the numerical method used to construct the magnetic field is described. From this, the basic structural form of the dips is presented in Section 3 and in Section 4 a possible origin of barbs is considered. The conclusions are then given in Section 5.

2. Assumptions and Numerical Method

Solar prominences or filaments may be described as long-lived regions of cool, dense material that are located in a much hotter and rarer coronal environment. Although they are much denser than their surroundings the plasma beta within prominences is still low ($\beta \sim 0.1-0.01$). This means that globally within a prominence the magnetic field plays a dominant role and plasma effects such as pressure and gravity may be neglected compared to magnetic effects. Prominences also have a very long lifetime and a slow global evolution, so that the global state may be described as being quasi-static. With these approximations the filaments magnetic field can be modelled with the force-free field approximation, in which the magnetic field threading through the prominence satisfies to zeroth order

$$\mathbf{j} \times \mathbf{B} = \mathbf{0}, \quad (1)$$

or

$$\nabla \times \mathbf{B} = \alpha \mathbf{B}, \quad (2)$$

$$\nabla \cdot \mathbf{B} = 0, \quad (3)$$

where α is a function of position and constant along any magnetic field line. To simplify the calculation only cases with $\alpha = \text{constant}$ will be considered so the computed structures are linear, force-free fields.

A structure will be considered suitable to represent a filament if it contains magnetic dips. When filaments are viewed on the solar disk they are seen in absorption and their shape is determined by cool plasma that sits in the dips. The plasma within these dips extends only to a height of roughly 1 pressure scale height (Priest, 1989). At prominence temperatures this is approximately at a height of 1 Mm. When the dips in the magnetic field are plotted they will only be shown up to a height of 1 Mm, thus simulating the region that would be observed if there were cool plasma sitting in the dips. By plotting the field lines in this manner, it is assumed that the cool plasma sits in the dips without deforming them greatly, which is a reasonable approximation.

To construct a 3-D linear ($\alpha = \text{constant}$) force-free equilibria Equation (2) must be solved subject to Equation (3). One method of doing this is to reduce the problem to one involving the vector potential \mathbf{A} ($\mathbf{B} = \nabla \times \mathbf{A}$), which is solved in a cube with sides ranging from $-L < x, y, z < L$. The equation

$$\nabla^2 \mathbf{A} + \alpha \nabla \times \mathbf{A} = 0, \quad (4)$$

is solved subject to the boundary conditions:

- (1) The tangential components of \mathbf{A} ($A_t = -\hat{\mathbf{n}} \times (\hat{\mathbf{n}} \times \mathbf{A})$) on each face are consistent with the prescribed normal component of \mathbf{B} ($B_n = \mathbf{B} \cdot \hat{\mathbf{n}}$);
- (2) The normal component of \mathbf{A} ($A_n = \mathbf{A} \cdot \hat{\mathbf{n}}$) satisfies $\nabla \cdot \mathbf{A} = 0$ on the boundary.

The cube represents an isolated region of the solar surface and flux can only enter or leave through the bottom surface ($z = -L$). This means that B_n , the normal component of \mathbf{B} , vanishes on each of the faces except $z = -L$ (which represents the photosphere). To satisfy boundary condition 1 it is assumed that the tangential components of \mathbf{A} are zero on each of the faces except $z = -L$. The second boundary condition may then be satisfied by having the normal derivative of the normal component of \mathbf{A} zero on each of these faces. If Equation (4) is solved subject to the above boundary conditions it is straight forward to show that the solution will have $\nabla \cdot \mathbf{A} = 0$ everywhere within the domain (Finn, Guzdar, and Uzikov, 1994). Thus this final equilibrium solution will correspond to the linear force-free field associated with the imposed normal field on the boundary with the choice of the Coulomb gauge ($\nabla \cdot \mathbf{A} = 0$).

The base flux now needs to be specified by choosing the normal component of the magnetic field ($B_n = B_z$) at $z = -L$. To do this it is first assumed that on the base

$$\frac{\partial A_z}{\partial z} = 0 \quad (5)$$

and conditions (1) and (2) give

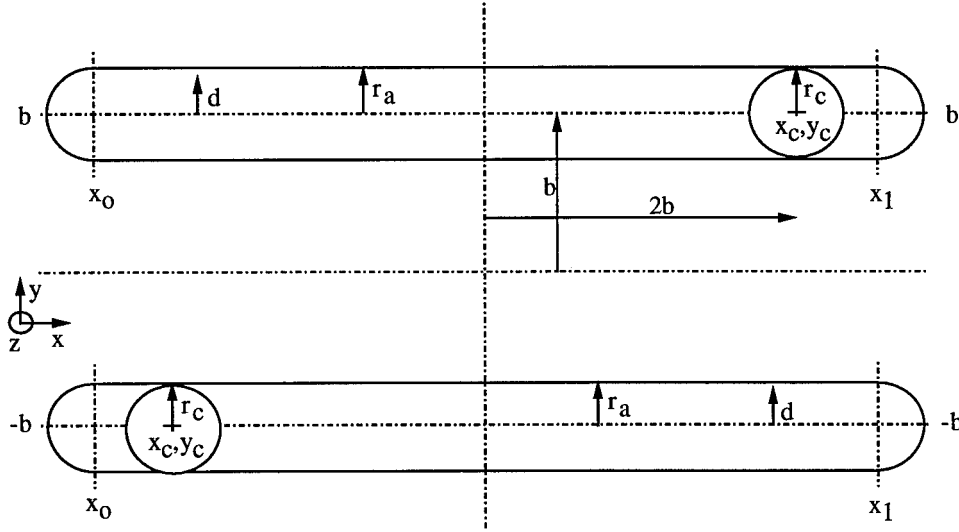


Figure 1. Schematic diagram of the location of sources and sinks in the channel.

$$B_z = \frac{\partial A_y}{\partial x} - \frac{\partial A_x}{\partial y}, \quad (6)$$

$$\frac{\partial A_z}{\partial x} + \frac{\partial A_x}{\partial y} = 0. \quad (7)$$

To find A_x , A_y on the base from B_z , the vector potential \mathbf{A} is written in the form of a flux function Φ such that

$$\mathbf{A} = \nabla \times (\Phi(x, y)\hat{\mathbf{z}}) + A_z\hat{\mathbf{z}}. \quad (8)$$

With this form for \mathbf{A} , Equation (6) becomes

$$\frac{\partial^2 \Phi}{\partial x^2} + \frac{\partial^2 \Phi}{\partial y^2} = -B_z.$$

This equation is then solved subject to the boundary conditions that

$$\frac{\partial \Phi}{\partial n} = 0 \quad (9)$$

on the boundaries ($x = \pm L$, $y = \pm L$). This is required so that on these boundaries the tangential components of \mathbf{A} go smoothly to zero. With A_x , A_y determined from B_z on the base the full problem can then be solved. In each case, the results are computed on a 129^3 grid. More details about the numerical method used can be found in the papers by Finn, Guzdar, and Uzikov (1994) and Longbottom, Fiedler, and Rickard (1998) and references therein.

An appropriate base flux configuration must now be chosen. Filaments are generally found to lie above bipolar flux distributions (Martin, 1990) so the base flux

configuration will take the form of a simple arcade but with an axial asymmetry in the arcade. This axial asymmetry gives a sinistral/dextral axial component to the photospheric flux in the channel (Figure 1). The flux distribution has two components, the first being the basic arcade structure given by a vertical component of field (\mathbf{B}_z) at $z = -L$ of

$$\begin{aligned} B_z &= \pm \frac{B_{0a}}{2} \left(1 + \cos \left(\frac{\pi d}{r_a} \right) \right), & x_0 < x < x_1, & 0 \leq d \leq r_a, \\ B_z &= \pm \frac{B_{0a}}{2} \left(1 + \cos \left(\frac{\pi r}{r_a} \right) \right), & x \leq x_0, x \geq x_1, & 0 \leq r \leq r_a, \end{aligned} \quad (10)$$

where x_0 and x_1 are the end-points of the flux region and B_{0a} its central strength. The arcade sources have a half width of r_a and are positioned at $y = \mp b$, where

$$\begin{aligned} d &= y \pm b, \\ r^2 &= (x - x_0)^2 + (y \pm b)^2, & x \leq x_0, \\ r^2 &= (x - x_1)^2 + (y \pm b)^2, & x \geq x_1. \end{aligned}$$

The axial component of the flux distribution is given by two circular regions of flux that lie at opposite ends of the arcade. These regions are added onto the flux of the arcade and the vertical component of field across them is given by

$$\begin{aligned} B_z &= \pm \frac{B_{0c}}{2} \left(1 + \cos \left(\frac{\pi r}{r_c} \right) \right), & 0 \leq r \leq r_c, \\ r^2 &= (x - x_c)^2 + (y - y_c)^2, \end{aligned} \quad (11)$$

where the region is centered at (x_c, y_c) and has a central strength of B_{0c} .

The positive arcade is placed at $y = -b$ and the negative arcade at $y = +b$ (Figure 1). The scaling is chosen so that $b = 1$ unit (30 000 km), i.e., the width of a supergranular cell on the quiet Sun. The ends of the arcade lie at $x_0 = -2.45$ and $x_1 = 2.45$ where the half-length of the numerical box is $L = 2.9$ units. Both dextral and sinistral axial components can be created depending on how the circular flux regions are placed in contrast to the arcades. In all cases the half-separation of the circular flux regions is taken to be twice that of the arcades so that a long thin channel is produced. When the positive circular region is placed at $x_c = -2$, $y_c = -b$ and the negative region is at $x_c = 2$, $y_c = b$ a dextral axial component is produced (Figure 1). However, if the sign of the x -coordinates is reversed a sinistral axial component is produced. The radius of both the circular region and the arcade region is set to be 0.29 units and only flux ratios of between $F_c/F_a = 0.0$ and 1.0 will be considered since a flux ratio greater than unity is unphysical. Once the field is computed for a specified α , each grid point is tested for the presence of dipoles. This occurs when the vertical component of field satisfies

$$B_z = 0 \quad (12)$$

and

$$B \cdot \nabla B_z > 0. \quad (13)$$

All of the grid points that satisfy this criterion are then used as the starting points for plotting field lines up to a maximum dip depth of 1 Mm. In the case where the dips are asymmetrical with one peak higher than the other the dipped region is only plotted to the depth of the lower peak (if it lies below 1 Mm) as it is only up to this height that material may be confined. In Aulanier and Démoulin (1998) the entire extent of the dips to a depth of 1 Mm is shown even if one peak is below this height but this does not show the true region over which mass may be held. From now on only the dextral channel as shown in Figure 1 will be considered.

3. Dipped Magnetic Field Configurations

Three-dimensional magnetic configurations are now computed for various flux ratios and values of alpha. Again, a magnetic configuration is considered suitable to represent a filament if it contains dips. Initially, a flux ratio of $F_c/F_a = 0.75$ and the dextral channel is considered. The values of alpha are changed to both positive and negative values and it is found that dextral filament structures only exist for negative values of alpha. Dips first occur for an alpha value of $-2.96 \times 10^{-8} \text{ m}^{-1}$, where the maximum allowable (or first resonant value) of alpha is around $-4.24 \times 10^{-8} \text{ m}^{-1}$. In Figure 2 the dips are viewed from above as they would be seen on the solar disk for three different alpha values. In each plot the dashed line represents the P.I.L. which is defined to be the location where $B_z = 0$ at a height of 0.045 units above the photosphere (1 grid point). The height of the dips are calculated from the photospheric surface ($z = -L$) and only dips that lie in the corona above a height of 0.1 units (3000 km) are considered. This is due to the fact that filaments exist in the corona and are observed in contrast with a much hotter and rarer coronal environment. Any dips at photospheric and chromospheric heights would be indistinguishable from surrounding material. With the field configuration used here dips also exist below a height of 0.1 units (3000 km) due to the fact that no background field component is included in the centre of the channel. In the Appendix it is shown that, when a background field component (such as exists everywhere on the Sun) is included, the dips at chromospheric heights are no longer formed, leaving only the ones at coronal heights.

In the first plot (Figure 2(a)) the value of alpha is $-3.21 \times 10^{-8} \text{ m}^{-1}$. A very thin region of dips lie in the centre of the channel above the P.I.L. and extend to a height of 0.23 units (7000 km) above the photosphere ($z = -L$). This value of alpha is close to the initial value for which the dips occur and therefore there is only a thin structure. It could, to some degree, resemble a very small microfilament. In

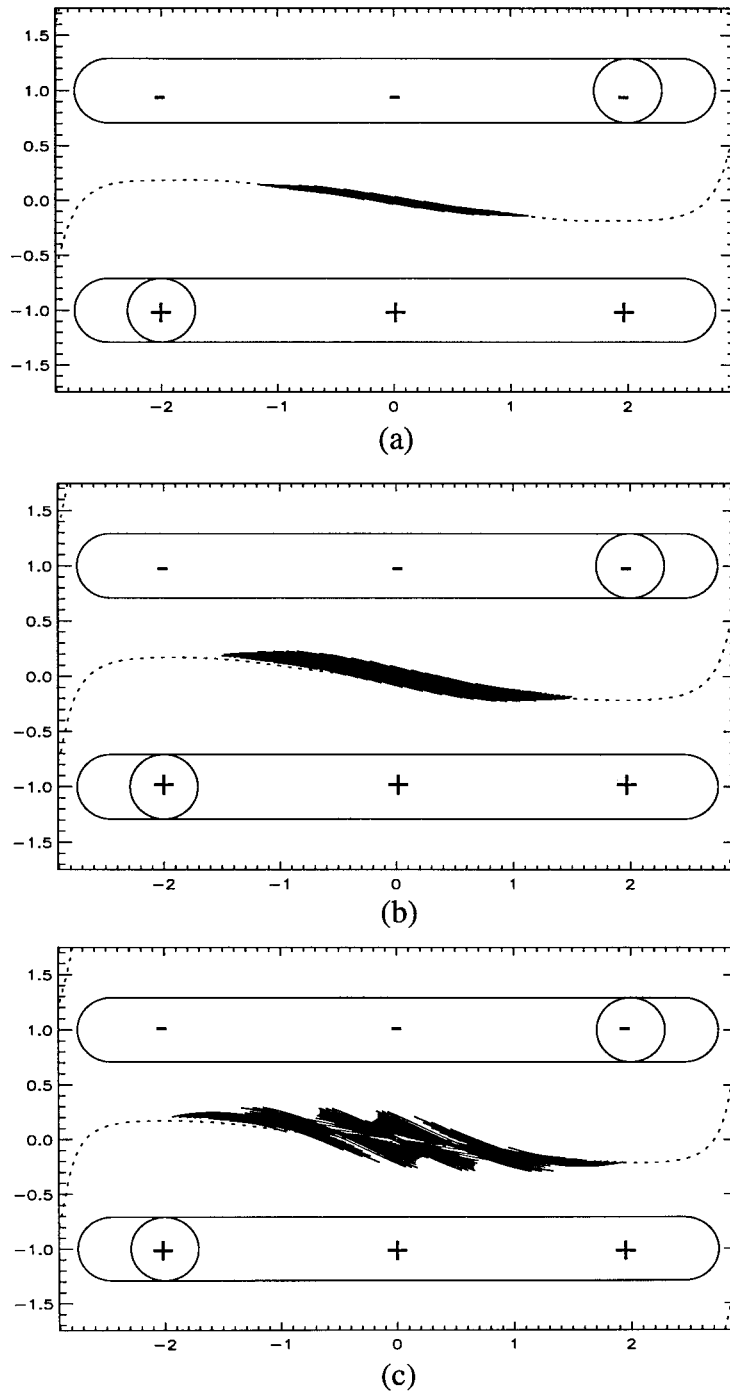


Figure 2. Extent of dipped region in the channel for (a) $\alpha = -3.21 \times 10^{-8} \text{ m}^{-1}$, (b) $-3.32 \times 10^{-8} \text{ m}^{-1}$, and (c) $\alpha = -3.55 \times 10^{-8} \text{ m}^{-1}$. The dashed line represents the P.I.L. and one unit in length corresponds to 30 000 km.

the next plot (Figure 2(b)) the value of alpha is changed to $-3.32 \times 10^{-8} \text{ m}^{-1}$ and it can be seen that there is a long thin region of dips in the centre of the channel again overlying the P.I.L. The dipped region is 3.3 units (100 000 km) in length and is roughly 0.17 units (5000 km) wide. The vertical extent of the dips is 0.5 units (15 000 km) above the photosphere. These dimensions are consistent with those observed for active-region filaments. When viewed from above the dips form a distinctive 'S'-type shape which is commonly associated with filaments and closely resembles a filament when seen on the disk in absorption. The ends of the dips are not located near any of the sources but lie in the centre of the channel. This means that the ends of the filament are not strictly associated with any flux regions, which is also a feature commonly observed in filaments.

The value of alpha is now changed to $-3.55 \times 10^{-8} \text{ m}^{-1}$ and the dips in the field lines are plotted in Figure 2(c). As before, with the increase in value of alpha more of the field lines are twisted along the channel and the region containing dips extends. The total length of the structure is now 4 units (120 000 km) and the thickness ranges from 0.1 units (3000 km) near the ends to 0.3 units (9000 km) in the centre. The vertical extent of the dips also increases with alpha and the dips now reach a height of roughly 1 unit (30 000 km). These dimensions are now comparable with those of a quiescent prominence. Since the structure varies by a factor of three in thickness from one end to the other this suggests that the entire body may be made up of a number of different strands. There are also some structures that branch out of the main axis and to the right. These structures could be associated with the barbs of filaments, however, their appearance is just due to the fact that not enough field lines are plotted to fill in the entire region of dips. Dips are found by testing the grid points to see if they satisfy Equations (12) and (13). However, since the calculation is done numerically with no analytical form for the field it is unlikely that $B_z = 0$ at any of the grid points. Condition (12) is replaced with the selection criteria that if $B_z/|B| \leq 0.01$ then the point may possibly be a dip. Condition (13) may then be used to validate this at the given grid point. When the selection criteria for choosing dips is relaxed the spaces between these branching structures fill up, so their appearance is just due to the selection criteria of choosing dips (i.e., the filling factor of field lines used).

In Figure 2 a large number of dips which lie at different heights and locations above the photosphere ($z = -L$) are superimposed on top of one another, so individual field lines cannot be seen and the structural form of the dips is not obvious. It is therefore useful to plot the extent of the dips at several different heights. This is done for alpha values of $-3.32 \times 10^{-8} \text{ m}^{-1}$ and $-3.55 \times 10^{-8} \text{ m}^{-1}$ since when alpha equals $-3.21 \times 10^{-8} \text{ m}^{-1}$ the dipped region is very thin and low-lying. The structural form of the dips is shown in Figure 3 where plots (a), (b) and (c) show the dips for $\alpha = -3.32 \times 10^{-8} \text{ m}^{-1}$ at heights of 0.2 units (6000 km), 0.29 units (8700 km) and 0.35 units (10 500 km) above the photosphere ($z = -L$), while (d), (e), and (f) show the dips for $\alpha = -3.55 \times 10^{-8} \text{ m}^{-1}$ at heights of 0.29 units (8700 km), 0.58 units (17 500 km) and 0.67 units (20 000 km), respectively. From

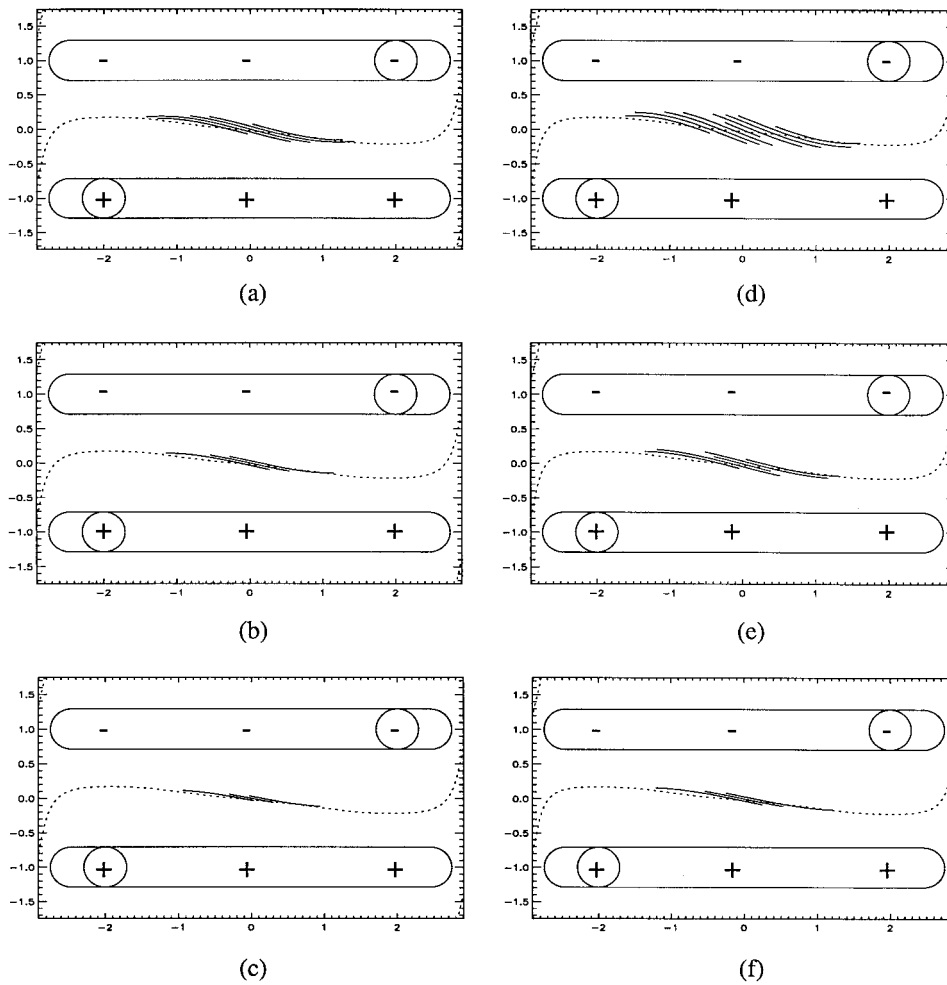


Figure 3. Structural form of the dipoles shown at heights of (a) 6000 km, (b) 8700 km, and (c) 10 500 km for $\alpha = -3.32 \times 10^{-8} \text{ m}^{-1}$ and heights of (d) 8700 km, (e) 17 500 km, and (f) 22 000 km for $\alpha = -3.55 \times 10^{-8} \text{ m}^{-1}$.

these plots the first thing to note is that none of the dipoles run along the entire length of the dipped region. In general they cut across the P.I.L. at some angle. The field lines for $\alpha = -3.55 \times 10^{-8} \text{ m}^{-1}$ cut across the P.I.L. at larger angles than those of $\alpha = -3.32 \times 10^{-8} \text{ m}^{-1}$. This is consistent with observations which show that the field in active-region filaments is more axial than in quiescent filaments. With increasing height the dipoles become more aligned with their long axis and their extent in the y -direction decreases. As a result the structures become thinner and more axial with height. As height increases the dipoles also become shallower and flatter. From this it can be seen that there are a large number of different field lines making

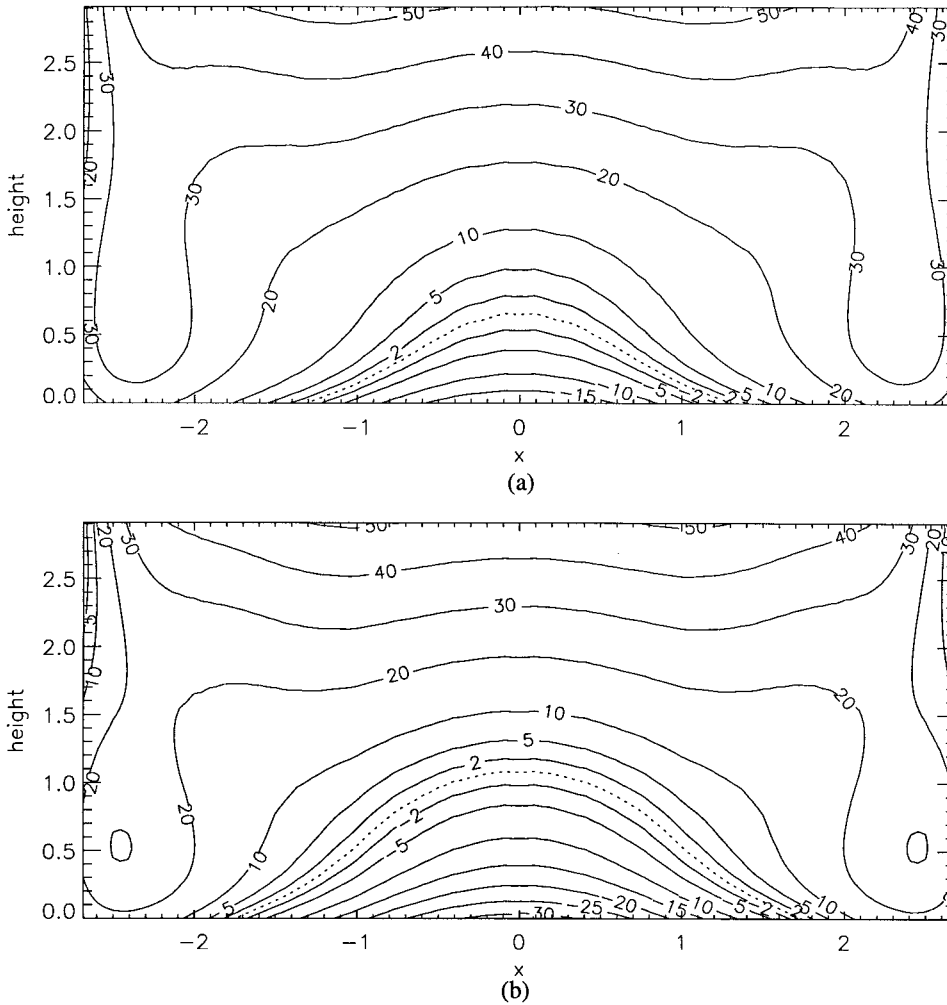


Figure 4. Skew angle of field lines in a vertical surface above the polarity inversion line for (a) $\alpha = -3.32 \times 10^{-8} \text{ m}^{-1}$ and (b) $\alpha = -3.55 \times 10^{-8} \text{ m}^{-1}$.

up each region of dips with all of the field lines lying at different angles and heights to each other.

In Figure 4 the variation of the skew angle of the field lines with height above the photosphere can be seen for (a) $\alpha = -3.32 \times 10^{-8} \text{ m}^{-1}$ and (b) $\alpha = -3.55 \times 10^{-8} \text{ m}^{-1}$. The contour plots are given in a vertical surface above the polarity inversion line, where the skew angle γ is the angle at which a field line cuts the upward projection of the photospheric polarity inversion line. Both plots extend to a height of 2.9 units (87 000 km) above the photosphere ($z = -L$). When γ is positive the field lines pass over in the 'normal' polarity direction and when it is negative they pass over in the 'inverse' polarity direction. The dashed line in each

of the plots denotes the location where the skew angle is zero and shows where the field lines are aligned with the polarity inversion line. In both cases there is a central region where the skew angle γ is negative (giving inverse polarity) and this outlines the location where the dips in the field lines lie. The magnitude of skew and the size of the region of ‘inverse’ polarity is much greater in Figure 4(b) than in 4(a) since the magnitude of α is larger. In both cases the skew angle in the region of dips is less than 30 deg and is consistent with observations of field angle measurements made within filaments. In both plots the skew gives a smooth transition with height and distance along the x -axis to positive values of γ which correspond to the arcades that overlie the dips. The skew of these arcades then increases with height. The contour plots show that the channel has a well defined magnetic orientation with height.

In prominences the magnetic field strength is observed to increase with height through the structure. Observations by Leroy, Bommier, and Sahal-Br  chot (1983) calculate the increase in field strength with height to be around $0.5 \times 10^{-4} \text{ G km}^{-1}$. In Figure 5 the variation of magnetic field strength with height for points above $x = 0, y = 0$ is shown for (a) $\alpha = -3.32 \times 10^{-8} \text{ m}^{-1}$ and (b) $\alpha = -3.55 \times 10^{-8} \text{ m}^{-1}$. In both plots it can be seen that in the region where the dips lie the magnetic field strength increases with height. Where the dips end the strength starts to decay away. The increase in field strength with height can be explained by considering the sign of the two terms that make up the Lorentz force. The Lorentz force may be decomposed into a magnetic tension force and magnetic pressure force such that

$$\mathbf{j} \times \mathbf{B} = (\mathbf{B} \cdot \nabla) \frac{\mathbf{B}}{\mu} - \nabla \left(\frac{B^2}{2\mu} \right). \quad (14)$$

For a force-free field the magnetic pressure force must balance the tension force everywhere. The z -component of the force-free equation gives

$$(\mathbf{B} \cdot \nabla) \frac{B_z}{\mu} - \frac{\partial}{\partial z} \left(\frac{B^2}{2\mu} \right) = 0. \quad (15)$$

At the location of the dips $(\mathbf{B} \cdot \nabla) B_z > 0$, and the tension force acts upwards. To balance this the pressure force must act downwards so $\partial/\partial z (B^2/(2\mu)) > 0$. In other words, the magnitude of the magnetic field must increase with height at the location of the dips or force balance will not occur. The results in Figure 5 are shown for a realistic arcade flux value of $1 \times 10^{21} \text{ Mx}$ ($B_{0\alpha} = 74 \text{ G}$) and the magnitude of the field in the dipped region lies around 23 G in Figure 5(a) and 25–27 G in Figure 5(b). In plot (a) the average increase in field strength with height is $0.3 \times 10^{-4} \text{ G km}^{-1}$ and in (b) $0.78 \times 10^{-4} \text{ G km}^{-1}$. These values are comparable with those found in Leroy, Bommier, and Sahal-Br  chot (1983). In this calculation the magnitude of the field strength may be slightly high but this is maybe due to the fact that linear force-free fields are being used. More accurate results may be found with non-linear force-free fields or a magnetostatic model both of which are much harder to construct.

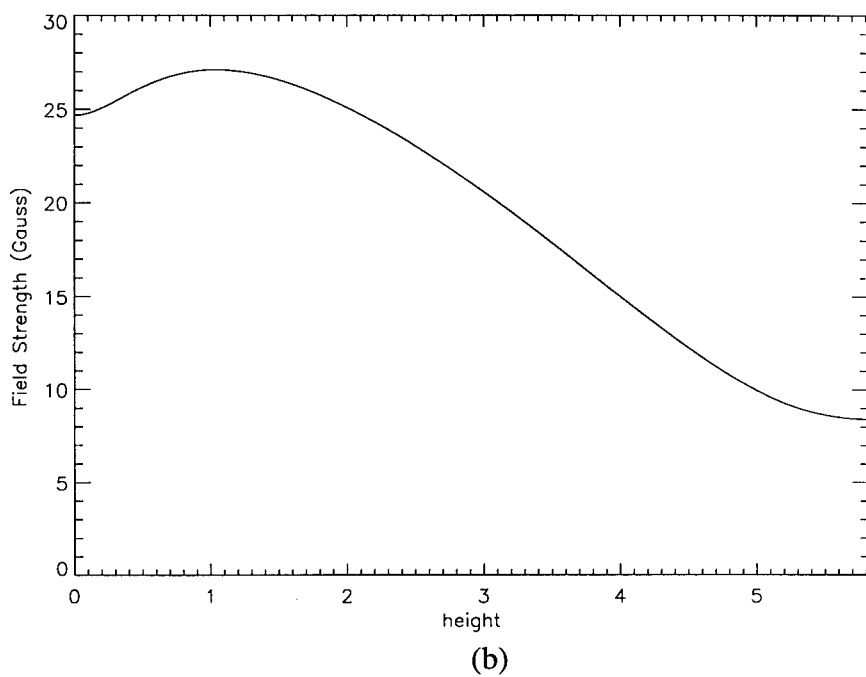
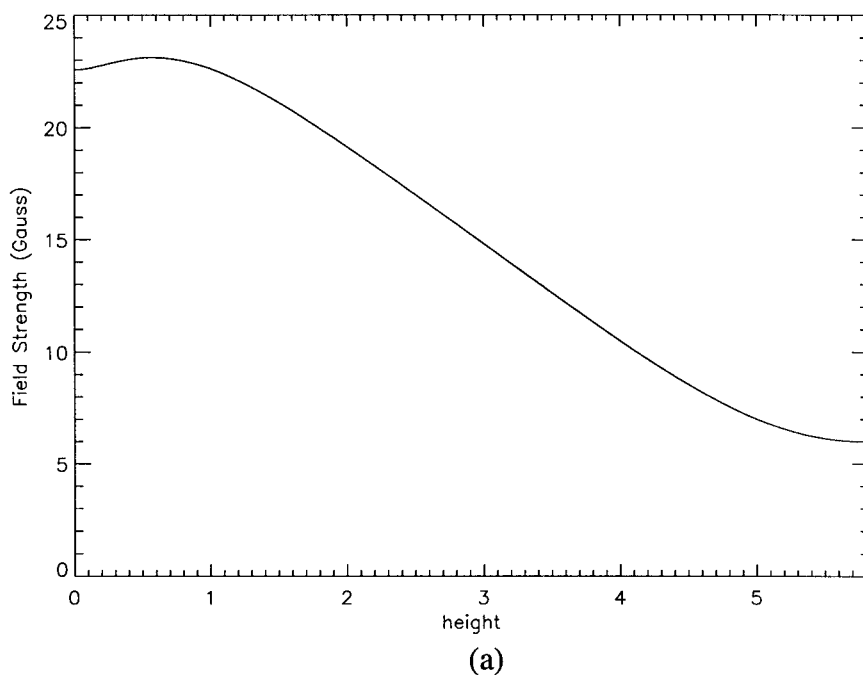
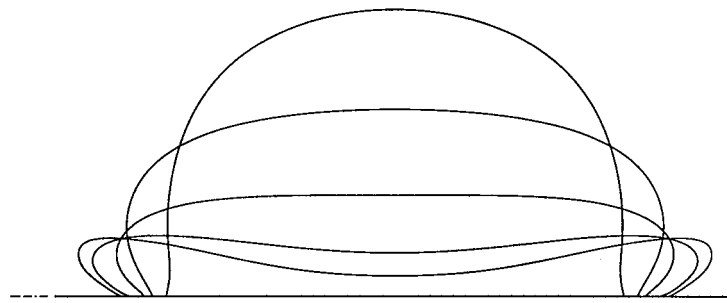
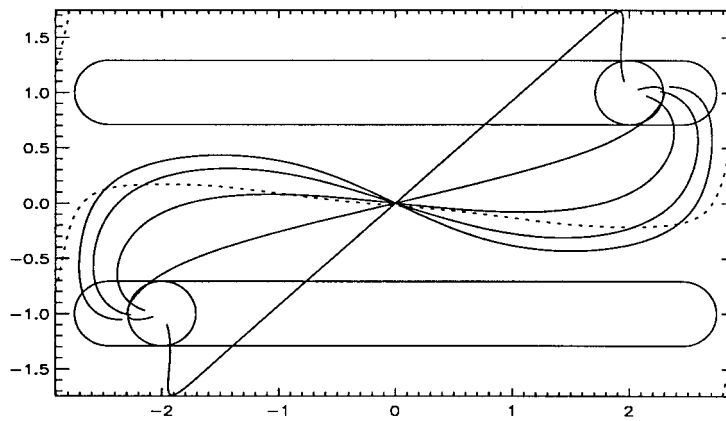


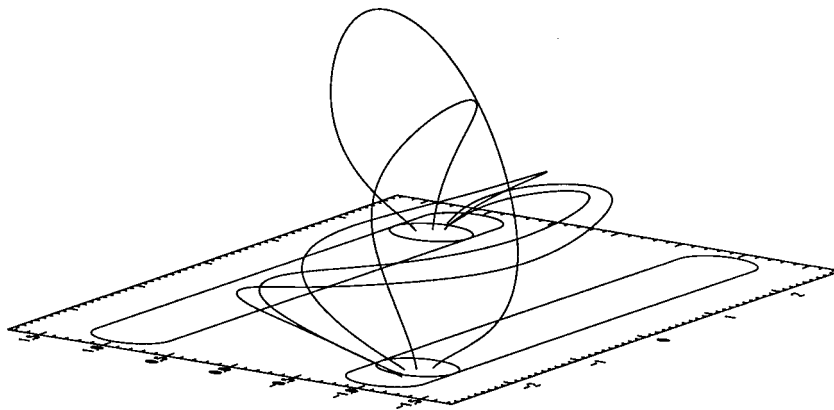
Figure 5. Magnetic field strength for points above $x = 0$, $y = 0$ for (a) $\alpha = -3.32 \times 10^{-8} \text{ m}^{-1}$ and (b) $\alpha = -3.55 \times 10^{-8} \text{ m}^{-1}$ for an arcade flux of $1 \times 10^{21} \text{ Mx}$ ($B_{0a} = 74 \text{ G}$).



(a)



(b)



(c)

Figure 6. Full length of field lines at heights of 6000 km, 13 000 km, 31 000 km, 57 000 km, and 87 000 km for $\alpha = -3.55 \times 10^{-8} \text{ m}^{-1}$ shown from (a) the side, (b) the top and (c) an oblique angle.

As well as showing the extent of the dips to a height of 1 Mm it is also useful to show the entire length of the field lines that are dipped. In Figure 6 the field lines in the channel are shown for $\alpha = -3.55 \times 10^{-8} \text{ m}^{-1}$ from (a) the side, (b) the top and (c) an oblique angle. The heights of the field lines above the photosphere ($z = -L$) are chosen to be 0.2 units (6000 km), 0.43 units (13 000 km), 1.03 units (31 000 km), 1.9 units (57 000 km) and 2.9 units (87 000 km), respectively. When the field lines are viewed from the side it can be seen that the two lowest field lines are dipped. As height increases, the dips become shallower and shallower and then they smoothly translate first onto flat field lines that lie above the dips and later onto large-scale arcades. When the same set of field lines are viewed from above the rotational shear in the field can be seen. In the plot the dashed line represents the P.I.L. and the field line with the largest negative skew has the biggest dip and is the lowest field line. The skew rotates in an anti-clockwise direction with height above the origin. Low down in the centre of the channel the field lines are of inverse polarity, which is consistent with the fact the fibrils which outline the field at low heights point away from the P.I.L. on either side of it. The very flat field lines that lie just above the dips run along a large length of the dipped region and these may be the structures that Solberg and McAllister (1998) observed to lie axially above filaments in X-rays when they become slightly disturbed. The arcades lying above the dextral filament are always left-bearing and have a rotational skew that is in the anti-clockwise sense with height. The opposite occurs for sinistral filaments and this is consistent with the observations of Martin and McAllister (1995). From the diagram it can be seen that there is a well defined magnetic structure with height above the channel. The structural form of the dips is very similar to that of Antiochos, Dahlburg, and Klimchuk (1995). All of the dipped field lines connect down to the photosphere and there are no disconnected helical flux rope type structures such as in Aulanier and Démoulin (1998).

When looking at the field lines from above the reason for the dips becomes apparent. In Figure 6(b) the dashed line denotes the location at a height of 0.045 units above the photosphere where $B_z = 0$. At this height and at all other heights above the channel from the bottom of the numerical box to the top similar lines can be drawn. This gives a surface extending up from the photosphere where $B_z = 0$. The two lowest field lines (which are the ones that are dipped) cut through this surface three times along their entire length, compared to once for the arcades. The dipped field lines pass through this surface twice in the normal polarity direction near their ends and once in the inverse polarity direction in the center of the channel. This can be seen by comparing how the field lines cut the dashed polarity inversion line in Figure 6(b). The polarity inversion line can be used as a good indication of the location of where $B_z = 0$ at higher heights as there is a good correlation between it and the surface of $B_z = 0$ when the surface is projected down onto the photosphere. This shows that B_z changes sign along the dipped field lines from positive-negative-positive and back to negative again and in doing so creates a dip in the centre. This can only occur for a linear force-free field when there is a large

enough twist in the field for the flux to be turned along the channel and back across the P.I.L. in the inverse direction. This type of field configuration is indicative of a filament channel, since the fibrils which lie at chromospheric heights always point away from the P.I.L. (in the inverse direction) on either side of the P.I.L. This type of configuration can only occur when a field is highly sheared, which is consistent with the observations of Schmieder *et al.* (1996).

Since filaments are relatively static objects the majority of the material contained within them must be held in static support against gravity by the magnetic field. Although most of the material is held in static support filaments are observed to have definite flows. The flow speeds in filaments are much less than the Alfvén velocity, so in general they do not affect the static field if they are directed along the field lines. Within filaments horizontal flows of around 5 km^{-1} are observed to run along the filament axis or spine. In Figure 6(b) all of the field lines connect down to the photosphere, so it is possible that material could be injected along them. The dipped field lines rotate in a counter-clockwise direction with height and in doing so become more axial with height. The higher up they are the shallower they become. For the higher field lines that are the shallowest and most axial the material would flow nearly horizontally along them such as has been observed by Sara Martin (private communication). The material could flow in either direction along the axial dips depending on the method that produces it. Possible methods are small-scale reconnections injecting material or pressure differences along the field line. The present topology is of a type that is consistent with the observed horizontal flows in filaments assuming that these flows are field aligned. Also when the field lines are viewed from certain angles, a limited helical structure can be seen along the region of dips. This is mainly a projection effect but it could explain why some helical flows are observed.

The range of values over which dipped magnetic field configurations exist must now be found. To begin with, a channel with a dextral axial component is considered with the flux locations shown in Figure 1. In Figure 7(a) the graph shows the range of parameter space over which dextral filament configurations exist. The x -axis gives the flux ratio and the y -axis the values of alpha (m^{-1}). Dextral filament configurations exist in between the two solid lines. The first solid line around $\alpha = -4.24 \times 10^{-8} \text{ m}^{-1}$ denotes the first resonant value of alpha where the magnetic energy and helicity become infinite for the linear force-free field and the second solid line denotes the point where the first dipped field line occurs as the field becomes more sheared. The dashed line shows where the dips become 1 Mm in depth. The first thing to note is that dextral filaments exist only for negative values of alpha and none exist for positive values of alpha. Also, very large values of alpha are required for dips to form and no dips occur around $\alpha = 0$, which is the potential case. As the flux ratio F_c/F_a increases, the range over which dips occur also increases. This is due to the fact that there is a stronger axial component of field in the channel. From this graph it can be seen that there is a small but definite

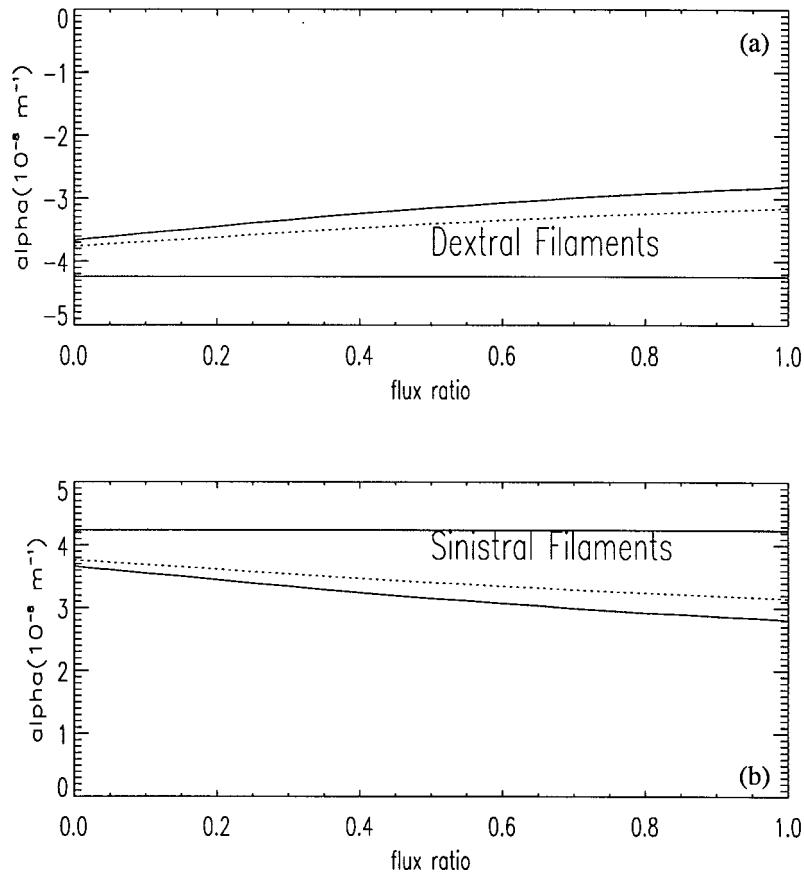


Figure 7. Range of parameter space over which dips occur for flux ratio against alpha for (a) a dextral channel and (b) a sinistral channel.

region of parameter space where magnetic configurations suitable for filaments exist. However, the region only occurs for large values of alpha.

The magnetic flux distribution is now changed so that the axial component of field in the channel is of sinistral type. This is done by placing the circular positive region at $x = 2, y = -1$ and the negative circular region at $x = -2, y = 1$. With this it is found that sinistral filaments exist only for positive values of alpha and the graph is shown in Figure 7(b). The graph, as expected, is the mirror image of the dextral one. It is interesting to note that when there is a pure arcade structure ($F_c/F_a = 0$) it is possible to obtain dips of dextral type for large negative values of alpha and of sinistral type for large positive values of alpha. The range of dips is very small but dips can be formed without there being an axial component of field in the channel from the photospheric flux distribution. In this case the axial component of field in the channel is purely a result of the sheared nature of the field

($\alpha \neq 0$). Even though dips can be formed without a photospheric axial component, having a photospheric axial component does help the production of dips.

One obvious question to ask from this is, ‘What happens when there is a dextral axial component from the flux distribution but a large positive value of alpha?’ In this case it is possible to obtain a sinistral dipped structure, if the twisting of the field is large enough to overcome the axial component due to the flux distribution. However, this is only possible for small flux ratios ($F_c/F_a < 0.2$) and large values of alpha ($\alpha > 4.01 \times 10^{-8} \text{ m}^{-1}$). Since the range of parameter space is very small and lies close to the resonant value of alpha it has not been included in the plots. By having a certain photospheric axial component of flux in the channel it is very difficult to form dipped structures of the opposite sense. It can be seen therefore that there is a definite region of parameter space in which filaments of a given type can exist. Dextral configurations exist only for negative values of alpha and sinistral ones for positive values of alpha (which was also found in Mackay, Priest, Gaizauskas, and van Ballegooijen (1998) and Auliner and Démoulin (1998)). This seems to indicate that the hemispheric pattern of filaments may be related to the hemispheric pattern in helicity, since helicity is predominately negative in the northern hemisphere and positive in the southern (Pevtsov, Canfield, and Metcalf, 1995).

4. Origin of Barbs

Filaments or prominences are observed to have structures that branch out from their main body and reach down to the chromosphere. These structures are called barbs and in dextral filaments they are always observed to be right-bearing and in sinistral filaments, left-bearing. Barbs are commonly associated with minority polarity regions of flux that lie on either side of the polarity inversion line. The nature of barbs and their link with minority polarity elements is now considered. To model barbs, small regions of flux are added into the channel and we explore the consequences of adopting the hypothesis that barbs form in dipped magnetic field lines. These elements are much weaker than the main arcades and their flux is taken to be one hundredth of the value of the arcade. The radius of each element is set to 0.12 units and the barbs are considered in a channel with a dextral axial component.

In Figure 8(a) the basic dipped structure of the field lines can be seen for $F_c/F_a = 0.5$ and $\alpha = -3.49 \times 10^{-8} \text{ m}^{-1}$. With no minority polarity regions of flux the structure is very similar to those obtained in the last section with the dips extending to a height of roughly 0.53 units (16 000 km) above the photosphere. There are no dipped field lines that branch off to the left or right from the main body. Small elements of flux are now added into the channel with the positive element added at $x = 0, y = 0.27$ and the negative element at $x = 0, y = -0.27$. By locating the positive polarity element on the negative polarity side of the P.I.L.

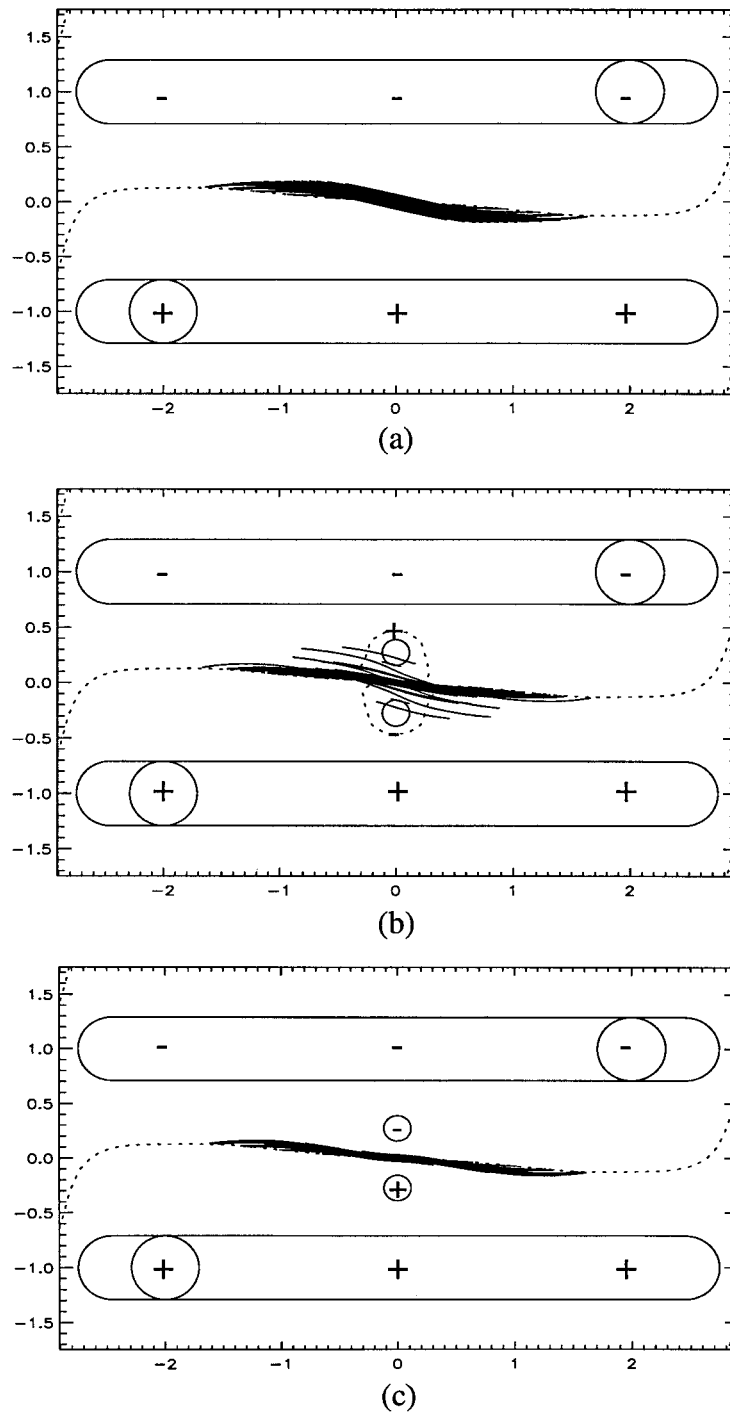


Figure 8. Link between barbs and the presence of small additional magnetic sources in the filament channel for $F_c/F_a = 0.5$, $\alpha = -3.49 \times 10^{-8} \text{ m}^{-1}$ showing (a) basic dipped structure, (b) barb-like structures created when the extra magnetic fragments have minority polarity and (c) the absence of barbs when the extra fragments have dominant polarity.

and the negative polarity element on the positive polarity side, minority polarity flux regions exist on either side of the P.I.L. The dips in the channel are now computed up to a height of 1 Mm and are shown in Figure 8(b). The presence of the minority polarity elements on either side of the P.I.L. causes a slight change to the global structure of the filament, however it is very similar to that previously calculated. The main changes occur in the centre of the channel, where dipped field lines branch out from the main body, due to the presence of the minority polarity elements. When viewed from both the positive polarity side and negative polarity side the dips bear off to the right from the main axis, which is correct for a dextral filament. These dips give a good representation of the barbs of filaments and connect from the lower half of the main body of the filament. By representing the barbs of filaments by dipped field lines the dextral filament in this model will always have right-bearing barbs and the sinistral filament correspondingly left-bearing barbs. This is a product of the direction of the field in the channel along with the sign changes of the field as it passes through the surface where $B_z = 0$ that lies above the P.I.L. that surrounds the minority polarity elements. A dip is formed when the vertical component of field changes from negative to positive. In Figure 8(b) this occurs before the flux passes over the positive polarity element and after it passes over the negative polarity element. It therefore gives an antiparallel alignment on either side of the filament and right-bearing barbs for the dextral filament. The mirror image of Figure 8(b) gives a sinistral filament with left-bearing barbs. As in Aulanier and Démoulin (1998) there are also a few dips that lie above the minority polarity elements but do not connect to the main axis of the filament. These structures also have an antiparallel alignment on either side of the P.I.L. Such dips could be described as fibrils that exist in the filament channel as they have the correct axial direction and point slightly away from the P.I.L. Most fibrils are, however, found around flux elements that have the same sign as the dominant flux on either side of the P.I.L. and therefore are probably caused by material being injected along flat or low-lying field lines. Fibrils only last for few hours and so are probably not stable enough to represent dipped magnetic field configurations.

In the final image (Figure 8(c)) the small fragments of flux on either side of the filament are changed to be of the same polarity as that of the arcades. When the dips are computed it is found that there are no structures that branch out of the main body and form dips. From this plot it can be seen that the structure of the filament has changed slightly from the case when no fragments were added. It is now much thinner and bends as it passes between the opposite polarity fragments, as shown in Priest, van Ballegoijen, and Mackay (1996). The flux from the small fragments just aligns itself with the pre-existing flux in the channel: no extra P.I.L.'s are created around them and no branching dipped structures are produced.

By assuming that barbs are produced by dipped field lines, Figure 8 shows that barbs of right-bearing structure can be reproduced for dextral filaments and barbs of left-bearing structure for sinistral filaments (mirror image of Figure 8(b)). The

barbs are only produced around minority polarity elements on either side of the P.I.L. due to the fact that these structures create an extra P.I.L. and corresponding surface above them where the sign of B_z can change from negative to positive and create a dip. No dipped structures are formed around flux elements that have the same polarity as that of the large scale arcades since no sign changes of B_z occur around them.

5. Conclusion

In this paper 3-D linear force-free field configurations that can be associated with filaments have been constructed. It is found that dipped magnetic field configurations can exist in a simple bipolar flux distribution but only for large values of alpha. The dipped field lines all connect down to the photosphere, as in Antiochos, Dahlburg, and Klimchuk (1995), and there are no isolated helical flux ropes, as found by Aulanier and Démoulin (1998). The dips are located in the centre of the channel above the polarity inversion line and when viewed from above to a depth of 1 Mm, they resemble to a remarkable degree filaments seen in absorption on the disk. The ends of the dips are located in the centre of the channel far from any flux regions. As the magnitude of alpha increases, the volume containing the dips also increases. For large values of alpha the volume of dips corresponds to the dimensions of a quiescent filament and for low values of alpha, active region filaments. Dextral filaments are found to exist only for negative values of alpha and sinistral filaments for positive values of alpha. Since there is a hemispheric pattern for alpha (Pevtsov, Canfield, and Metcalf, 1995), with alpha predominately negative in the northern hemisphere and positive in the southern, this suggests that the hemispheric pattern of filaments may just be a result of the hemispheric pattern of helicity. Studies which follow the development of helicity over the solar cycle, as flux is pushed from low to high latitudes, would be required to demonstrate this.

The field lines that are dipped are all of inverse polarity and cut the P.I.L. at an angle that is less than 30° , which is consistent with magnetic field measurements. In the dipped regions no dips run along the entire length of the region and each region is made up of a large number of dips which lie at different angles to each other at different heights. This is the type of magnetic configuration that would be required to give the fibril like appearance of some filaments. Another observed feature of filaments that is reproduced by the model is the increase in field strength with height (Leroy, Bommier, and Sahal-Bréchet, 1983). The increase only occurs in the region where the field lines are dipped, since an increasing field strength with height is required to balance the upwards tension force of the force-free magnetic field. Although the field lines low down in the channel are of inverse polarity, the arcades that lie above them are of normal polarity. For dextral filaments they are left-bearing when viewed from above and for sinistral filaments they are right-bearing, which is consistent with observations. Also the field lines in

the channel have an anti-clockwise rotation with height for dextral filaments and a clockwise rotation with height for sinistral filaments. This is again consistent with observations.

The origin of mass within filaments has been a major question facing filament research for many years. In this paper each grid point that is found to be a dip is used as the starting point to plot a field line up to a depth of 1 Mm simulating the effect of cool dense material lying in the dip. In reality, however, there is no reason why all of the field lines should contain cool dense material. Many methods have been suggested for the origin of the cool dense material and include (1) lifting of subphotospheric mass into the corona (Rust and Kumar, 1995), (2) Ballistic injection of chromospheric material into the corona (An, Bao, and Wu, 1986) and (3) evaporation and condensation of chromospheric material (Antiochos and Klimchuk, 1991). In a recent paper Dahlburg, Antiochos, and Klimchuk (1998) it has been shown that a substantial cool coronal condensation can be created in a dipped configuration if there is a localised heating near the footpoints of the field lines. Since there is no reason why the heating should occur on all of the field lines some of them may not contain cool material. This could lead to the appearance of a number of different structures of the filament within one magnetic configuration depending on which field lines are heated. An example of the type of configuration that could be produced can be seen in Figure 2(c) where branching structures are seen on either side of the P.I.L. due to the fact that not enough field lines have been plotted to fill the gaps between them. Also the appearance of barbs around minority polarity elements in Figure 8(b) would also depend on the dipoles containing cool material.

With the basic flux components of the channel, in general, however there are no dipoles that branch out of the main region of dipoles and resemble barbs when the entire region of dipoles is filled in. To model barbs when the entire region of dipoles is filled in, minority polarity flux regions have to be added into the channel and we have used the hypothesis that barbs are associated with dipped field lines. With this hypothesis, right-bearing barbs form for dextral filaments and left-bearing barbs for sinistral filaments. Barbs may form above the minority polarity elements since when these elements are added new polarity inversion lines are created around them. This allows the sign of B_z to change from negative to positive and produce a dip. This, however, only occurs on one side of the element as the flux passes over them. It occurs before the flux passes over the positive polarity element and after it passes over the negative polarity element and therefore gives the correct right-bearing/left-bearing structure for dextral/sinistral filaments and an anti-parallel alignment on either side of the P.I.L. No barbs are formed around ordinary polarity elements since they cause no sign change of the vertical field around them and therefore they do not create a dip. By considering barbs as dipped field lines the correct observational structural properties can be found. This model shows that many of the main observational properties of filaments and their barbs can be produced simply with a linear force-free field when it is highly sheared.

Appendix. Background Field Component

A background field component is now added in the channel in order to see how the previous results are changed when a more realistic flux distribution is used. It is found that when the background field is added in the centre of the channel the dips that existed at chromospheric heights can be removed leaving only the ones at coronal heights.

The flux distribution used in Section 2 is taken but this time a constant component of field is added between the two main flux regions. In Figure 9(a) a plot of the vertical component of magnetic field at $z = -L$ can be seen along the $x = 0$ line. This shows the basic flux components without the axial component due to the circular regions of flux. It can be seen that the field strength between the arcades does not fall to zero as in the previous case but is roughly $\frac{1}{15}$ the peak strength of the main arcades. When a network flux of 1×10^{21} Mx is used, $B_{0a} = 74$ G and the strength of the background field is ± 5 G everywhere, which is consistent with observed values. The channel is now constructed as before for a flux ratio of $F_c/F_a = 0.75$ and an alpha value of $3.4375 \times 10^{-8} \text{ m}^{-1}$ which lies in the middle of the previous range of values.

The grid points are again tested for dips and each dip is plotted up to a depth of 1 Mm and viewed from above in Figure 9(b). It can be seen that there is a long thin region of dips that lie in the centre of the channel above the polarity inversion line. The dipped region is roughly 2.4 units (72 000 km) long and extends from 0.1 unit (3000 km) to 0.55 units (16 000 km). The structure is 0.1 units (3000 km) thick. The plot denotes a very long, thin, tall region of dips. No dips lie below a height of 3000 km, which represents chromospheric heights. Although the vertical extent of the dipped region is very similar the width of it is much less than before. This is because the background field keeps the region of dips confined in the centre of the channel. However, the same form of solution is obtained as before with just a slightly differing configuration due to the different flux distribution.

In the next plot (Figure 9(c)) the skew angle of the field lines can be seen, defined in the same manner as before. Again the dashed line denotes the region where the skew angle is zero, with the field lines aligned with the polarity inversion line. Again there is a central region where the skew angle is negative and this outlines the region of dips. In contrast to the previous examples, the channel is not of inverse polarity at chromospheric heights. The region of inverse polarity forms an isolated region which does not extend down to the photosphere. At low heights there are normal polarity field lines with a skew of around 5° . Since they are of normal polarity the field lines at these heights are not dipped. The size of the region of inverse polarity increases as the magnitude of alpha increases and, when enough twist is added, the region extends down to the photosphere. The region of inverse polarity can also be made smaller or larger by varying the strength of the background field.

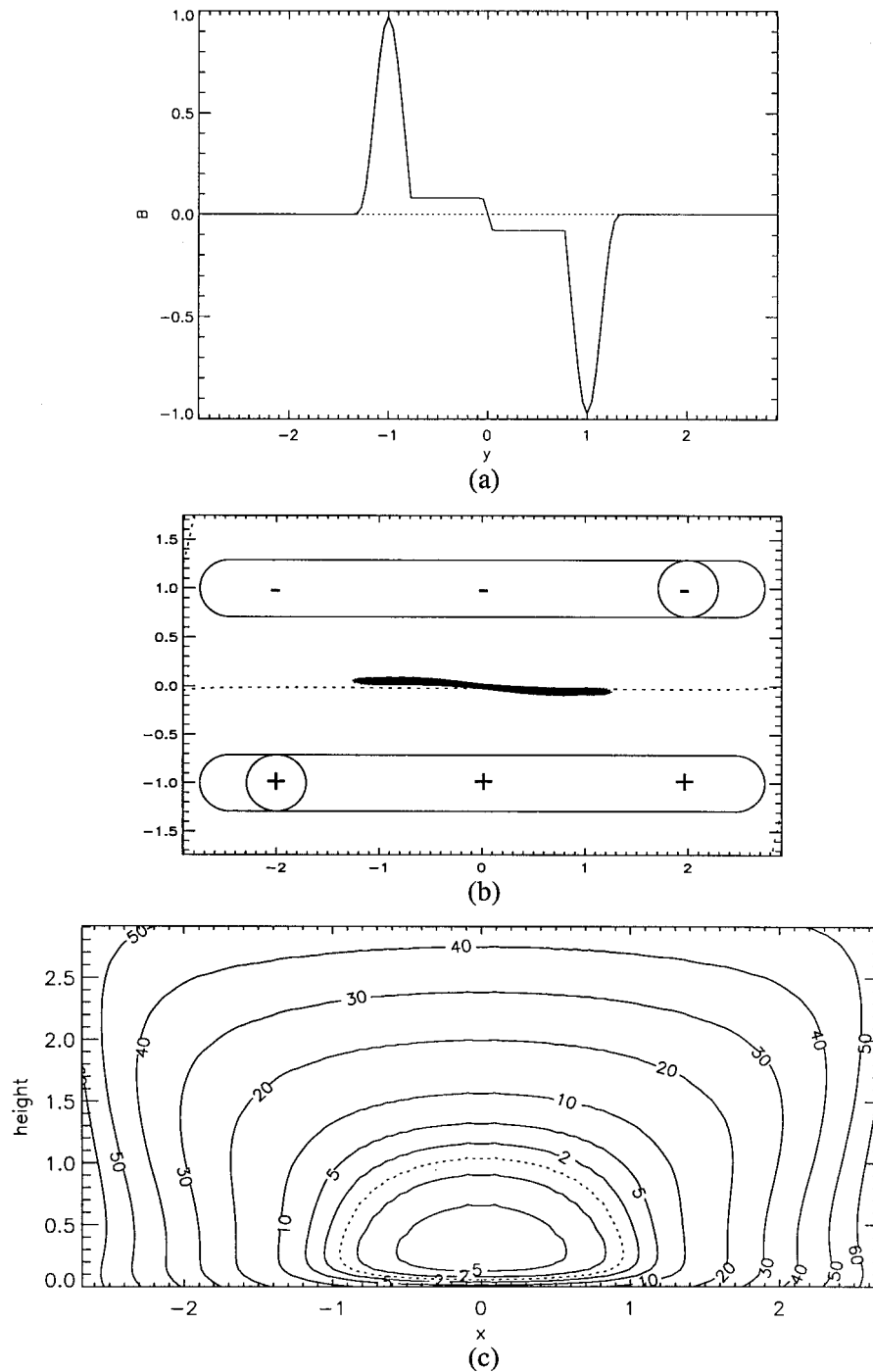


Figure 9. (a) Cut in y -direction of vertical field component in channel at $z = -l$ when a background field component is added. (b) Region of dips for $F_c/F_a = 0.75$ and $\alpha = 3.4375 \times 10^{-8} \text{ m}^{-1}$ and (c) a skew angle of field lines in a surface above the P.I.L. showing disconnected region of inverse polarity when the background field is added.

From this it can be seen that when a background field component is added to the channel such as exists on the Sun, there are no longer any dips at chromospheric heights. The principle behind the solution is exactly the same as before but with a slight modification of the configuration due to the extra field components. A large number of different solutions can be produced depending on the exact flux distribution used but the solutions always obey the same principle that dipped field lines can occur for large values of α .

Acknowledgements

The authors would like to thank Alan Hood, Terry Forbes, Thomas Neukirch, Klaus Galsgaard, Vic Gaizauskas, and Pascal Démoulin for helpful discussions. The 129^3 grid point solutions were computed on the J90 at the Rutherford Appleton Laboratory and financial support for the work was given by the UK Particle Physics and Astronomy Research Council.

References

- An, C. H., Bao, J. J., and Wu, S. T.: 1986, in A. Poland (ed.), *Coronal and Prominence Plasmas*, (NASA CP-2442), Washington, GPO), p. 51.
- Antiochos, S. K. and Klimchuck, J. A.: 1991, *Astrophys. J.* **378**, 372.
- Antiochos, S. K., Dahlburg, R. B., and Klimchuck, J. A.: 1995, *Astrophys. J.* **420**, L41.
- Athay, R. G., Querfeld, C. W., Smartt, R. N., Landi degl'Innocenti, E., and Bommier, V.: 1983, *Solar Phys.* **89**, 3.
- Aulanier, G. and Démoulin, P.: 1998, *Astron. Astrophys.* **329**, 1125.
- Bommier, V. and Leroy, J. L.: 1997, 'New Perspectives on Solar Prominences', *IAU Colloq.* **167**.
- Dahlburg, R. B., Antiochos, S. K., and Klimchuck, J. A.: 1998, *Astrophys. J.* **495**, 485.
- Foukal, P.: 1971, *Solar Phys.* **19**, 59.
- Finn, J. M., Guzdar, P. N., and Usikov, D.: 1994, *Astrophys. J.* **427**, 475.
- Hood, A. W. and Anzer, U.: 1990, *Solar Phys.* **126**, 117.
- Kippenhahn, R. and Schlüter, A.: 1957, *Z. Astrophys.* **43**, 36.
- Kuperus, M.: 1996, *Solar Phys.* **169**, 349.
- Kuperus, M. and Raadu, M. A.: 1974, *Astron. Astrophys.* **31**, 189.
- Leroy, J. L., Bommier, V., and Sahal-Bréchet, S.: 1983, *Solar Phys.* **83**, 135.
- Longbottom, A. W., Fiedler, R. A. S., and Rickard, G. J.: 1998, *Astron. Astrophys. Suppl.*, in preparation.
- Mackay, D. H., Priest, E. R., Gaizauskas, V., and van Ballegoijen, A. A.: 1998, *Solar Phys.* **180**, 299.
- Martin, S. M.: 1990, 'Dynamics of Quiescent Prominences', *Proc. IAU Colloq.* **117**, *Lecture Notes in Physics* **363**, Springer-Verlag, New York, p. 1.
- Martin, S. M., Bilimoria, R., and Tracadas, P. W.: 1994, in R. J. Rutten and C. J. Schrijver (eds.), *Solar Surface Magnetism*, Springer-Verlag, New York, p. 303.
- Martin, S.F., and McAllister, A.H.: 1995, *Bull. Amer. Astron. Soc.* **27**, 961.
- Pevstov, A. A., Canfield, R. C., Metcalf, T. R.: 1995, *Astrophys. J.* **440**, L109.
- Priest, E. R.: 1989, *Dynamics and Structure of Quiescent Solar Prominences*, Kluwer Academic Publishers, Dordrecht, Holland.

- Priest, E. R., Van Ballegoijen, A., and Mackay, D. H.: 1996, *Astrophys. J.* **460**, 530.
- Querfeld, C. W., Smartt, R. N., Bommier, V., Landi degl'Innocenti, E., and House, L. L.: 1985, *Solar Phys.* **96**, 277.
- Rust, D. M. and Kumar, A.: 1995, *Solar Phys.* **155**, 69.
- Schmieder, B., Démoulin, P., Aulanier, G., and Golub, L.: 1996, *Astrophys. J.* **467**, 881.
- Solberg, F. C. R. and McAllister, A.: 1998, in D. Webb, D. Rust, and B. Schmieder (eds.), 'New Perspectives on Solar Prominences', *IAU Colloq.* **167**, ASP Conference Series, p. 171.
- Tandberg-Hansen, E.: 1974. *Solar Prominences*, D. Reidel Publ. Co., Dordrecht, Holland.
- Zirker, J. B., Martin, S. F., Harvey, K., and Gaizauskas, V.: 1997, *Solar Phys.* **175**, 24.